Journal of Engineering Mathematics **39:** 3–24, 2001.

Shear flow over a particulate or fibrous plate

C. POZRIKIDIS
Department of Mechanical and Aerospace Engineering University of California, San Diego, La Jolla, California 92093-0411, U.S.A. (e-mail: cpozrikidis@ucsd.edu, Internet URL: http://stokes.ucsd.edu/c_pozrikidis)

Received: 15 September 1999, accepted in revised form 10 April 2000

Abstract. Simple shear flow over a porous plate consisting of a planar array of particles is studied as a model of flow over a membrane. The main objective is to compute the slip velocity defined with reference to the velocity profile far above the plate, and the drift velocity induced by the shear flow underneath the plate. The difference between these two velocities is shown to be proportional to the thickness of the plate. When the geometry of the particle array is anisotropic, the directions of the slip and drift velocity are generally different from the direction of the overpassing shear flow. An integral formulation is developed to describe flow over a plate consisting of a periodic lattice of particles with arbitrary shape, and integral representations for the velocity and pressure are developed in terms of the doubly-periodic Green's function of three-dimensional Stokes flow. Based on the integral representation, asymptotic expressions for the slip and drift velocity are derived to describe the limit where the particle size is small compared to the inter-particle separation, and numerical results are presented for spherical and spheroidal particles of arbitrary size. The asymptotic results are found to be accurate over an extended range of particle sizes. To study the limit of small plate porosity, the available solution for shear flow over a plane wall with a circular orifice is used to describe flow over a plate with a homogeneous distribution of circular perforations, and expressions for the slip and drift velocity are derived. Corresponding results are presented for axial and transverse shear now over a periodic array of cylinders arranged distributed in a plane. Streamline pattern illustrations confirm that a negative drift velocity is due to the onset of eddies between closely-spaced particles.

Key words: Stokes flow, integral equations, shear flow, porous plate, membrane.

1. Introduction

An important area of research in biomechanics concerns the effect of a shear flow on the equilibrium shapes of, and mass transport through, membranes enclosing vesicles and biological cells [1–3]. The membranes typically consist of lipid bilayers, sometimes resting on a network of proteins comprising the cytoskeleton, separating the vesicle or cytoplasmic fluid from the ambient plasma or buffer fluid. From the point of view of hydrodynamics, a membrane may be regarded as a screen or sieve, and the problem of flow through or over it may be studied within the more general context of flow over a porous or irregular plate separating two semi-infinite regions occupied by the same or different fluids. This more general problem is pertinent to several other areas of biofluiddynamics and mainstream engineering fluid mechanics involving, for example, flow over arrangements of cilia or bundled tubes.

Previous studies of the thermodynamics and hydrodynamics of polymeric and biological membranes have modeled the network of the fundamental molecular units comprising a membrane as a planar lattice of particles over which the smaller molecules of the solute slide [4, 5]. The theory seeks to predict the species diffusivity and to establish the relationship between the pressure drop and the geometrical properties of the membrane expressed in terms of the hydrodynamic resistance for flow normal to the membrane. Ishii [6] studied flow normal to

a planar lattice of spherical particles in the asymptotic limit where the particle size is small compared to the particle separation. To the author's knowledge, shear flow over a porous plate or particulate plane has not been addressed explicitly by previous authors, although three related classes of problems have been discussed in detail.

The first class of problems involves flow over an irregular surface with small or large amplitude protuberances possibly of fractal nature [7, 8]. Issues of interest include the establishment of the physical origin of the no-slip boundary condition, the computation of the slip velocity as a function of the morphology of the surface irregularities, and the study of transport properties in terms of effective heat or mass transfer coefficients. The second class of problems involves shear flow over a semi-infinite particulate matrix modeling a porous medium. Reviews and numerical simulations for two- and three-dimensional arrangements were presented by Larson and Higdon [9, 10] and Sangani and Behl [11]. Their results illustrated the dependence of the slip velocity on the geometry of the porous medium microstructure, and helped to establish a theoretical foundation for Brinkman's equation governing the structure of the flow near the surface of a porous medium, also pointing out its limitations. The third class of problems involves shear flow over a wall with a circular hole or side pore, possibly in the presence of suction that drives the fluid through the hole or into the pore, with applications to particle entrainment and particle screening [12–15].

In this paper, we study shear flow over a planar lattice of particles forming a porous surface. When the thickness of the plate is comparable to, or larger than, the gaps between the particles, regions of recirculating flow develop in the intervening spacing, and the flow decays rapidly underneath the array to give a virtually quiescent lower fluid. When, however, the particle size is smaller than the inter-particle separation, the shear flow penetrates the lower fluid, and a uniform drift velocity is established underneath the array. If the particle shape or lattice geometry is anisotropic, the direction of the drift velocity is generally different from that of the overpassing shear flow. Far above the lattice, the flow reduces to simple shear flow with a macroscopic slip velocity similar to that established in shear flow over a porous material. The main goal of the present work is to illustrate the dependence of the slip and drift velocity on the particle shape and lattice geometry.

The asymptotic and numerical studies are based on integral representations of periodic Stokes flow using an appropriate Green's function. In implementing the numerical procedure for solving an integral equation of the first kind for the traction over a particle surface, a general method is developed for removing the eigenfunction of the single-layer Stokes hydrodynamic potential. To complement the results for three-dimensional flow over a planar array, two related configurations are also considered. The first configuration involves shear flow over a flat plate of zero thickness containing a homogeneous distribution of circular perforations of small size, which is relevant to shear flow over a porous plate with a large solid areal fraction. The second configuration involves longitudinal and transverse shear flow over an array of cylinders. Comparisons of the results for three-and two-dimensional configurations illustrate once again the fundamental differences in the nature of the corresponding flows.

2. Shear flow over a planar particle lattice

Consider infinite simple shear flow over a two-dimensional lattice of identical rigid particles positioned at the vertices of a regular lattice that is parallel to the xy plane, as shown in

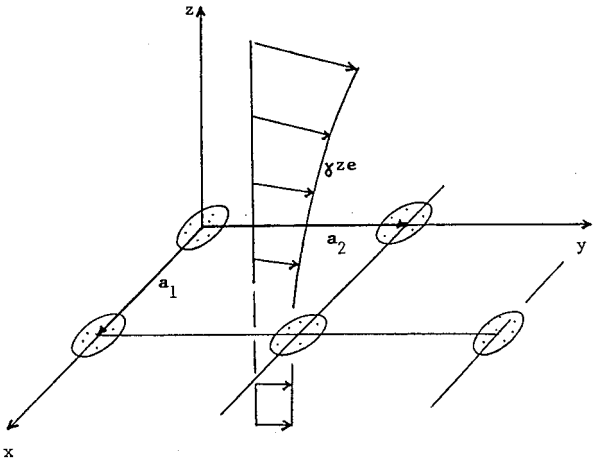

Figure 1. Shear flow over a planar lattice of particles. Far below the lattice, the velocity tends to the uniform drift velocity whose direction and magnitude are determined by the particle shape and size, the lattice geometry, and the direction of the shear flow.

Figure 1. The lattice is described by two base vectors $\mathbf{a}_1$ and $\mathbf{a}_2$, so that the designated centers of two particles labelled n and m are related by

$$\mathbf{X}_n = \mathbf{X}_m + i_1\mathbf{a}_1 + i_2\mathbf{a}_2, \tag{1}$$

where i_1 and i_2 are two integers.

Far above the lattice, as z tends to $+\infty$, the flow reduces to simple shear flow with shear rate γ in the direction of the unit vector $\mathbf{e}$ that is parallel to the xy plane. Thus, the slope of the velocity is required to exhibit the asymptotic behavior

$$\lim_{z\to+\infty} \frac{\mathrm{d}\mathbf{u}}{\mathrm{d}z} \to \gamma\mathbf{e} \tag{2}$$

while the pressure tends to a constant value denoted by $p^{+\infty}$. Far below the lattice, as z tends to $-\infty$, the shear stress is required to vanish,

$$\lim_{z\to-\infty} \frac{\mathrm{d}\mathbf{u}}{\mathrm{d}z} \to 0 \tag{3}$$

and the pressure tends to a constant value denoted by $p^{-\infty}$. Integration of the preceding two equations with respect to z produces the asymptotic forms

$$\lim_{z\to+\infty} \mathbf{u} \to \gamma z\mathbf{e} + \mathbf{U}^{+\infty} + \mathrm{edt} \tag{4}$$

and

$$\lim_{z\to-\infty} \mathbf{u} \to \mathbf{U}^{-\infty} + \mathrm{edt}, \tag{5}$$

where $\mathbf{U}^{+\infty}$ and $\mathbf{U}^{-\infty}$ are two constant velocities parallel to the xy plane, both to be computed as part of the solution, and 'edt' stands for exponentially decaying terms. The magnitude and direction of the slip velocity $\mathbf{U}^{+\infty}$ depend on the definition of the origin of the z axis; in the present case, the origin coincides with the designated particle centers [9, 16]. The magnitude and direction of the uniform drift velocity induced by the shear flow under the lattice, $\mathbf{U}^{-\infty}$, on

the other hand, is independent of the origin of the z axis. Neither the slip velocity nor the drift velocity is necessarily oriented in the direction of the shear flow. In practice, the shear flow may be generated by the translation of a flat plate located at $z = z_p$ with velocity $\mathbf{U}_p$ parallel to the particle lattice. Using the asymptotic form (4), we find $\mathbf{U}_p = \gamma z_p \mathbf{e} + \mathbf{U}^{+\infty}$, which provides us with an expression for evaluating $\gamma\mathbf{e}$ and $\mathbf{U}^{+\infty}$, when another linear relationship between them has been established.

Returning to the problem of infinite shear flow, we perform a force balance over a control volume that is confined between (*a*) four planes that are perpendicular to the xy plane and enclose one lattice cell and thus one particle, (*b*) two planes that are parallel to the xy plane located far above or below the particle lattice, and (*c*) the surface of the enclosed particle, to obtain

$$\mathbf{F} \equiv \int_{\text{Particle}} \mathbf{f}(\mathbf{x})\, \mathrm{d}S(\mathbf{x}) = \mu\gamma A\mathbf{e} + A(p^{-\infty} - p^{+\infty})\mathbf{e}_z, \tag{6}$$

where $\mathbf{F}$ is the force exerted on one particle, $\mathbf{f} = \sigma \cdot \mathbf{n}$ is the hydrodynamic traction, σ is the stress tensor, $\mathbf{n}$ is the unit vector normal to the particle pointing into the fluid, μ is the fluid viscosity, A is the area of one lattice cell, and $\mathbf{e}_z$ is the unit vector pointing along the z axis.

The motion of the fluid is governed by the equations of Stokes flow [17]

$$\nabla p = \mu\nabla^2\mathbf{u}, \qquad \nabla \cdot \mathbf{u} = 0 \tag{7}$$

which are to be solved subject to (a) the far-field conditions expressed by Equations (4) and (5), (b) the no-slip and no-penetration condition $\mathbf{u} = \mathbf{0}$ on the particle surface, and (c) the periodicity condition

$$\mathbf{u}(\mathbf{x}) = \mathbf{u}(\mathbf{x} + i_1\mathbf{a}_1 + i_2\mathbf{a}_2) \tag{8}$$

where i_1 and i_2 are two integers. Our main objective is to compute the slip and drift velocities as functions of the particle shape and size and of the lattice geometry, in the limit of vanishing Reynolds number.

2.1. Integral formulation

To prepare the ground for the integral formulation, we introduce the Green's function of the equations of Stokes flow describing the doubly-periodic flow due to a two-dimensional lattice of point forces that is identical to the particle lattice shown in Figure 1. The velocity and pressure field induced by the point forces at the point $\mathbf{x}$ are expressed by

$$u_1(\mathbf{x}) = \frac{1}{8\pi\mu} G_{ij}(\mathbf{x}, \mathbf{x}_0)\, b_j, \qquad p(\mathbf{x}) = \frac{1}{8\pi} P_j(\mathbf{x}, \mathbf{x}_0)\, b_j \tag{9}$$

where $\mathbf{G}$ is the velocity Green's function tensor, $\mathbf{P}$ is the pressure Green's function vector, and $\mathbf{b}$ is the strength of a point force; one arbitrarily selected point force is located at $\mathbf{x}_0$. The Green's functions for the velocity and pressure satisfy the periodicity condition shown in Equation (8). Moreover, as $z - z_0$ tends to $+\infty$, we require the asymptotic behavior

$$\lim_{z\to+\infty} \mathbf{G}(\mathbf{x}, \mathbf{x}_0) \to -\frac{8\pi}{A}(z - z_0)\, \mathbf{J} + \text{edt}, \qquad \lim_{z\to+\infty} \mathbf{P}(\mathbf{x}, \mathbf{x}_0) \to \frac{8\pi}{A}\mathbf{e}_z + \text{edt}, \tag{10}$$

where $\mathbf{J}$ is the identity matrix but with the third diagonal component corresponding to the z axis set equal to zero. As $z - z_0$ tends to $-\infty$, all components of the Green's functions are

required to vanish. When the point forces are parallel to the lattice, the pressure field decays far from the lattice. When the point forces are perpendicular to the lattice, a pressure difference is established across the lattice to balance the point force exerted on the volume of fluid confined within each periodic cell.

The computation of the Green's functions in terms of Fourier series or Ewald sums has been discussed by Ishii [6], Sangani and Behl [11], and Pozrikidis [18]. As the observation point $\mathbf{x}$ approaches a point force, the expressions in terms of Fourier series converge extremely slowly and are inadequate for the purposes of numerical computation. As an alternative, we evaluate the Green's function using the fast summation method developed in [18], based on the expression

$$\begin{aligned}\mathbf{G}(\mathbf{x},\mathbf{x}_0) \;=& \sum_n \left(\mathbf{I}\frac{1-3\xi r_n+\xi^2 r_n^2}{r_n}+(\mathbf{x}-\mathbf{x}_n)(\mathbf{x}-\mathbf{x}_n)\frac{1+\xi r_n-\xi^2 r_n^2}{r_n^3}\right)\mathrm{e}^{-\xi r_n}+\\ &+\frac{4\pi}{A}\sum_{\substack{m\\ |\mathbf{l}_m|\neq 0}}(-\mathbf{I}\nabla^2+\nabla\nabla)\\ &\frac{1}{2}\left(\frac{1+\rho_m}{|\mathbf{l}_m|^3}\mathrm{e}^{-\rho}+\frac{(2-\zeta_m^2)(1+\delta\sqrt{1+\zeta_m^2})+\delta^2(1+\zeta_m^2)}{\xi^3(1+\zeta_m^2)^{5/2}}\right)\cos(\mathbf{l}_m\cdot\mathbf{x})+\\ &+\frac{4\pi}{A}(-\mathbf{I}\nabla^2+\nabla\nabla)\frac{2+2\delta+\delta^2}{2\xi^3}\mathrm{e}^{-\delta}\cos(\mathbf{l}_m\cdot\mathbf{x})\end{aligned} \tag{11}$$

where ξ is an arbitrary splitting parameter, $r_n=|\mathbf{x}-\mathbf{x}_n|$, $\mathbf{x}_n$ is the location of the nth point force, the first sum on the right-hand side of (11) runs over all point forces, and the second sum runs over the nodes of the reciprocal planar wave number lattice with base vectors $\mathbf{b}_1=(2\pi/A)\mathbf{a}_2\times\mathbf{e}_z$ and $\mathbf{b}_2=(2\pi/A)\mathbf{e}_z\times\mathbf{a}_1$; $\rho_m=|\mathbf{l}_m|(z-z_0)$, $\zeta_m=|_m|/\xi$, and $\delta=\xi(z-z_0)$. The computations reported in later sections were conducted using $\xi=2\pi/\sqrt{A}$. Figure 2(a) shows the streamline pattern in the xz plane induced by a square lattice of point forces directed along the x axis. The unit lattice vectors are given by $\mathbf{a}_1=(L,0,0)$, $\mathbf{a}_2=(0,L,0)$, and one of the point forces is located at the origin, The onset of regions of recirculating flow above and below the lattice is a dominant feature of the motion.

It can be shown that, subject to the previously stated conditions, the Green's function satisfies the properties

$$\mathbf{G}(\mathbf{x},\mathbf{x}_0)=\mathbf{G}(\mathbf{x}_0,\mathbf{x})-\frac{8\pi}{A}(z-z_0)\,\mathbf{J} \tag{12}$$

and

$$\mathbf{P}(\mathbf{x},\mathbf{x}_0)=\mathbf{P}(\mathbf{x}_0,\mathbf{x})-\frac{8\pi}{A}\mathbf{e}_z \tag{13}$$

which allow us to switch the location of the singular point and field point, provided that we also include a complementary shear flow or decrease the pressure by an appropriate amount.

Considering now the control volume confined between (a) four planes that are perpendicular to the xy plane and enclose one lattice cell and thus one particle, (b) two planes that are parallel to the xy plane and are located far above or below the particle lattice, and (c) the surface of the enclosed particle, we use the integral representation for Stokes flow to express

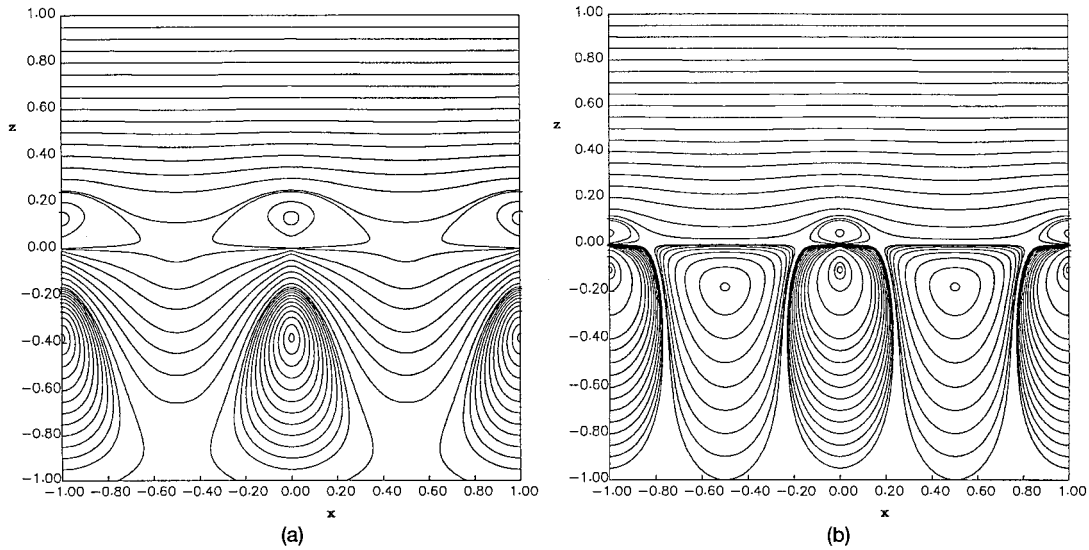

Figure 2. (a) Streamline pattern in the xz plane induced by a square lattice of three-dimensional point forces directed along the x axis. (b) Streamline pattern induced by an array of two-dimensional point forces directed along the x axis.

the flow variables in terms of boundary integrals [17]. Exploiting the stipulated periodicity of the flow and the conforming periodicity of the Green's function, shifting the bottom boundary of the control volume to negative infinity, and noting that far below the lattice the velocity of the shear flow tends to a constant value whereas the Green's function for the velocity vanishes, we derive the following representation for the velocity at a point $\mathbf{x}_0$:

$$u_j(\mathbf{x}_0) = -\frac{1}{8\pi\mu}\int_{\text{Particle}} G_{ij}(\mathbf{x},\mathbf{x}_0)\, f_i(\mathbf{x})\, \mathrm{d}S(\mathbf{x}) + \\ +\frac{1}{8\pi\mu}\int_{\text{Top}} G_{ij}(\mathbf{x},\mathbf{x}_0)\, f_i(\mathbf{x})\, \mathrm{d}S(\mathbf{x}) - \frac{1}{8\pi}\int_{\text{Top}} n_i(\mathbf{x}) T_{ijk}(\mathbf{x},\mathbf{x}_0) u_k(\mathbf{x})\, \mathrm{d}S(\mathbf{x}) \tag{14}$$

where $\mathbf{T}$ is the stress tensor associated with the Green's function, and "Top" denotes the top of the control volume. Over the particle surface, the unit normal vector $\mathbf{n}$ points into the fluid, whereas over the top of the control volume, $\mathbf{n}$ points toward the positive z axis. Observing the limit as the top of the control volume moves to infinity, and noting the asymptotic behavior of the flow under consideration and of the periodic Green's function, we obtain a simplified representation in terms of the single-layer Stokes potential and the unknown slip velocity,

$$u_j(\mathbf{x}_0) = -\frac{1}{8\pi\mu}\int_{\text{Particle}} G_{ij}(\mathbf{x},\mathbf{x}_0)\, f_i(\mathbf{x})\, \mathrm{d}S(\mathbf{x}) + \gamma z_0\, e_j + U_j^{+\infty}. \tag{15}$$

Taking now the limit as the field point $\mathbf{x}_0$ moves far below the particle array, and using the asymptotic behavior of the Green's function described earlier, we find

$$U_j^{-\infty} \to -\frac{1}{8\pi\mu}\left(-\frac{8\pi}{A}\right)\int_{\text{Particle}} (z - z_0) J_{ij}\, f_i(\mathbf{x})\, \mathrm{d}S(\mathbf{x}) + \gamma z_0 e_j + U_j^{+\infty}. \tag{16}$$

Breaking up the integral into two parts, and using the integral force balance expressed by equation (6), we obtain a relationship between the slip and drift velocities,

$$U_j^{-\infty} = U_j^{+\infty} + J_{ij}\frac{1}{\mu A}\int_{\text{Particle}} z f_i(\mathbf{x})\,\mathrm{d}S(\mathbf{x}) \tag{17}$$

which shows that their difference is on the order of the particle size normal to the lattice. For discoidal particles of zero thickness, the difference will vanish.

It is both useful and physically appealing to recast the representation (15) into an alternative form expressing the flow induced by a distribution of point forces over the particle surfaces. For this purpose, we use identity (12) to switch the arguments of the Green's function, finding

$$\begin{aligned} u_j(\mathbf{x}_0) = & -\frac{1}{8\pi\mu}\int_{\text{Particle}} G_{ji}(\mathbf{x}_0,\mathbf{x}) f_i(\mathbf{x})\,\mathrm{d}S(\mathbf{x}) + J_{ij}\int_{\text{Particle}} (z-z_0) f_i(\mathbf{x})\,\mathrm{d}S(\mathbf{x}) + \\ & + \gamma z_0 e_j + U_j^{+\infty}. \end{aligned} \tag{18}$$

The first integral on the right-hand side of (18) represents the requisite distribution of point forces. To simplify the remaining terms, we use an integrated form of the reciprocal relation for Stokes flow over the boundaries of the control volume previously defined, written for the flow under consideration and for a test shear flow with velocity $\mathbf{u}^{\text{test}} = \gamma^{\text{test}}(z-z_0)\mathbf{e}^{\text{test}}$, where γ^{test} is an arbitrary shear rate and $\mathbf{e}^{\text{test}}$ is an arbitrary unit vector parallel to the xy plane, obtaining

$$\int_{\text{Particle, Bottom, Top}} \gamma^{\text{test}}(z-z_0) e_i^{\text{test}} f_i(\mathbf{x})\,\mathrm{d}S(\mathbf{x}) = \int_{\text{Particle, Bottom, Top}} u_i(\mathbf{x}) f_i^{\text{test}}(\mathbf{x})\,\mathrm{d}S(\mathbf{x}). \tag{19}$$

Requiring the boundary condition at the particle surface, shifting the top and bottom boundaries of the control volume far above or below the particle lattice, and taking into consideration the asymptotic behavior of the flow, we obtain the identity

$$\int_{\text{Particle}} (z-z_0) f_j(\mathbf{x})\,\mathrm{d}S(\mathbf{x}) = -\mu\gamma A z_0 + \mu\gamma^{\text{test}} A(U_i^{-\infty} - U_i^{+\infty}). \tag{20}$$

Finally, we combine equations (18–20) and derive the desired representation

$$u_j(\mathbf{x}_0) = -\frac{1}{8\pi\mu}\int_{\text{Particle}} G_{ji}(\mathbf{x}_0,\mathbf{x}) f_i(\mathbf{x})\,\mathrm{d}S(\mathbf{x}) + U_j^{-\infty}. \tag{21}$$

On the basis of this representation, we find that pressure difference across the lattice is given by

$$p^{-\infty} - p^{+\infty} = \frac{1}{A}\mathbf{F}\cdot\mathbf{e}_z \tag{22}$$

in agreement with (6).

Evaluating equation (15) or (21) at the particle surface, and requiring the boundary condition $\mathbf{u} = \mathbf{0}$, we obtain a Fredholm integral equation of the first kind for the distribution of the traction $\mathbf{f}$. Equation (6) provides us with a supplementary condition that we may use to compute the slip velocity $\mathbf{U}^{+\infty}$ or drift velocity $\mathbf{U}^{-\infty}$. Having computed one, the other follows from Equation (17).

2.2. Multiple arrays

The formulation for shear flow over a two-dimensional particle array developed in this section may be extended readily to shear flow over multiple arrays or a semi-infinite lattice modeling an ordered porous medium, considered by Sangani and Behl [11]. In the case of flow over a semi- infinite lattice, the fast decay of the velocity down the lattice causes the drift velocity to vanish, yielding the counterpart of the representation (21)

$$u_j(\mathbf{x}_0) = -\frac{1}{8\pi\mu}\sum_{l=1}^{\infty}\int_{P_l} G_{ji}(\mathbf{x}_0,\mathbf{x})\, f_i(\mathbf{x})\, \mathrm{d}S(\mathbf{x}) \tag{23}$$

where P_l denotes a particle that belongs to the lth array. Evaluating this representation at a point located on a particles surface, and requiring the boundary condition $\mathbf{u} = \mathbf{0}$, we obtain a homogeneous Fredholm integral equation of the first kind for the distribution of the traction $\mathbf{f}$, which is to be solved subject to a constraint imposed by the x and y components of the integral force balance

$$\sum_{l=1}^{\infty}\int_{P_l} \mathbf{f}(\mathbf{x})\, \mathrm{d}S(\mathbf{x}) = \mu\gamma A\mathbf{e} + A(p^{-\infty} - p^{+\infty})\mathbf{e}_z. \tag{24}$$

The pressure drop across the lattice arises as part of the solution in terms of the z component of the force exerted on the individual particles.

3. Asymptotics for small particles

When the typical particle size a is small compared to the characteristic dimension of the particle lattice L, an approximate solution of the problem posed in Section 2 may be found using the method of matched asymptotic expansions. Considering the integral representation (21), we find that, to leading order with respect to the small parameter $\varepsilon = a/L$, the velocity induced at the designated center of one particle by all other particles is given by

$$u_j(\mathbf{x}_p) \cong \frac{1}{8\pi\mu} D_{ji} F_i + U_j^{-\infty}, \tag{25}$$

where $\mathbf{D}$ is the difference between the free-space Green's function or Stokeslet, denoted by $\mathbf{S}$, and the periodic Green's function, evaluated at the particle center $\mathbf{x}p$,

$$D_{ji} \equiv (S_{ji} - G_{ji})(\mathbf{x}_p, \mathbf{x}_p). \tag{26}$$

Using the principles of matched asymptotic expansions, we find that to leading order in ε, the force exerted on the particle is given by

$$F_k \cong 6\pi\ \mu\ a\ R_{kj}\Big(\frac{1}{8\pi\mu}\ D_{ji}F_i + U_j^{-\infty}\Big), \tag{27}$$

where $\mathbf{R}$ is a dimensionless resistance tensor relating the force exerted on a stationary solitary particle to the velocity of an infinite uniform incident flow. For a spherical particle of radius a, $\mathbf{R}$ is the identity matrix $\mathbf{I}$. Solving Equation (27) for $\mathbf{U}^{-\infty}$, and using expression (6) to evaluate the force, we obtain

$$\mathbf{U}^{-\infty} \cong \frac{\gamma A}{6\pi a}(\mathbf{R}^{-1} - \tfrac{3}{4}a\ \mathbf{D})\cdot\mathbf{e} \tag{28}$$

accurate to first order with respect to ε. An alternative form of (28) is

$$\mathbf{U}^{-\infty} \cong \frac{1}{6}\gamma a\frac{1}{\phi}\left(\mathbf{R}^{-1} - \tfrac{3}{4}\phi^{1/2}\left(\frac{A}{\pi}\right)^{1/2}\mathbf{D}\right)\cdot\mathbf{e}, \tag{29}$$

Table 1. Diagonal components of the matrix **D** for a rectangular lattice of side ratio δ.

δ	LD_{xx}	LD_{yy}	LD_{zz}
0·1	−13·02	33·95	6·98
0·2	−13·44	3·11	−3·44
0·3	−11·67	− 3·33	−5·00
0·4	−10·19	− 5·38	−5·18
0·5	− 9·04	− 6·09	−5·04
0·6	− 8·14	− 6·29	−4·81
0·7	− 7·41	− 6·27	−4·56
0·8	− 6·81	− 6·14	−4·32
0·9	− 6·30	− 6·01	−4·10
1·0	− 5·85	− 5·85	−3·90

where $\phi = \pi a^2/A$ is the effective areal fraction of the planar array occupied by the particles.

Expression (28) illustrates the singular behavior of the drift velocity, and thus of the slip velocity, in the limit as the particle size becomes much smaller than the particle separation. Physically, the small surface area of the particles requires a large incident velocity to produce a force that is able to balance the shear stress exerted at the top of the lattice. This singular behavior is analogous to that exhibited by the velocity of a non-deforming three-dimensional particle lattice upon which a constant force is exerted due, for example, to gravity [19]. Moreover, expression (28) illustrates that when, either the resistance tensor for the force, or the Green's function tensor **D**, or both, are anisotropic, the drift velocity, and thus the slip velocity, is not necessarily directed parallel to the shear flow; that is, a shear flow in a certain direction may cause a drift or slip velocity in another direction.

For a rectangular lattice with base vectors $\mathbf{a}_1 = L(1, 0, 0), \mathbf{a}_2 = L(0, \delta, 0)$ parallel to the x or y axis, where δ is the dimensionless aspect ratio, the matrix $\mathbf{D}(\mathbf{x}_p, \mathbf{x}_p)$ is diagonal. Numerical computation produces the values of the diagonal components listed in Table 1 in terms δ. The values of D_{zz} are implicit in a graph presented by Ishii ([6] Figure 2), and agree with the present results within plotting resolution. It is interesting to note the inversion in the sign of D_{yy} and D_{zz} for small lattice aspect ratios; the physical interpretation of this behavior is not clear. For a hexagonal lattice corresponding to $\mathbf{a}_1 = L(1, 0, 0), \mathbf{a}_2 = L(0{\cdot}5, 3^{1/2}/2, 0)$, the tensor $\mathbf{D}(\mathbf{x}_p, \mathbf{x}_p)$ is diagonal with components $D_{xx} = D_{yy} = 6{\cdot}32/L$, and $D_{zz} = 4{\cdot}21/L$.

3.1. Shear flow over a semi-infinite lattice

The preceding asymptotic solution may be extended readily to shear flow over multiple particle arrays. The extension to a semi-infinite lattice, considered previously by Sangani and Behl [11] using a somewhat different method, requires modification due to the vanishing of the drift velocity. For simplicity, we assume that all particle layers are identical, and the layer separations are constant and equal to H.

As the particle size becomes smaller than the inter-particle separation, the integral representation (23) evaluated at the center of a particle located at the kth layer, yields

$$u_i(\mathbf{x}^{(k)}) \cong \frac{1}{8\pi\mu} D_{ij}(\mathbf{x}^{(k)}, \mathbf{x}^{(k)}) F_j^{(k)} - \frac{1}{8\pi\mu} \sum_{\substack{l=1 \\ l\neq k}}^{\infty} G_{ij}(\mathbf{x}^{(k)}, \mathbf{x}^{(l)}) F_j^{(l)}, \tag{30}$$

where $\mathbf{F}^{(m)}$ is the force exerted on a particle the belongs to the mth layer, and the tensor $\mathbf{D}$ is defined in (26). A global force balance requires

$$\sum_{l=1}^{\infty} \mathbf{F}^{(l)} = \mu\gamma A\, \mathbf{e} + A\,(p^{-\infty} - p^{+\infty})\, \mathbf{e}_z. \tag{31}$$

Using the method of asymptotic expansions, we find

$$\mathbf{F}_m^{(k)} = 6\pi\mu a\, \mathbf{R}_{mi} \left[\frac{1}{8\pi\mu} D_{ij}(\mathbf{x}^{(k)}, \mathbf{x}^{(k)}) F_j^{(k)} - \frac{1}{8\pi\mu} \sum_{\substack{l=1 \\ l\neq k}}^{\infty} G_{ij}(\mathbf{x}^{(k)}, \mathbf{x}^{(l)}) F_j^{(l)} \right], \tag{32}$$

where $\mathbf{R}$ is the resistance tensor for the force exerted on a particle in infinite uniform flow. Rearranging Equation (32), we obtain the homogeneous linear system

$$\left(\mathbf{I} - \frac{3}{4} a\, \mathbf{R} \cdot \mathbf{D}(\mathbf{x}^{(k)}, \mathbf{x}^{(k)}) \right) \cdot \mathbf{F}^{(k)} + \frac{3}{4} a\, \mathbf{R} \cdot \sum_{\substack{l=1 \\ l\neq k}}^{\infty} \mathbf{G}(\mathbf{x}^{(k)}, \mathbf{x}^{(l)}) \cdot \mathbf{F}^{(l)} = \mathbf{0} \tag{33}$$

which is to be solved subject to the global constraint imposed by (31). Recalling the linear dependence of the Green's function for the velocity on the vertical coordinate z far above a plane of the point forces, we derive the approximate form

$$\left(\mathbf{I} - \frac{3}{4} a\, \mathbf{R} \cdot \mathbf{D}(\mathbf{x}^{(k)}, \mathbf{x}^{(k)}) \right) \cdot \mathbf{F}^{(k)} - \frac{6\pi a}{A}\, \mathbf{R} \cdot \sum_{l=k+1}^{\infty} (z^{(k)} - z^{(l)}) \mathbf{J} \cdot \mathbf{F}^{(l)} = \mathbf{0} \tag{34}$$

which is a generalization of the asymptotic form of Equation (59) derived by Sangani and Behl [11] for spheres.

To establish the asymptotic behavior far below the top layer, we note that the solution of the discrete problem expressed by Equation (34) bears some resemblance to the solution of the integral equation

$$\left(\mathbf{I} - \tfrac{3}{4} a\, \mathbf{R} \cdot \mathbf{D}(\mathbf{x}^{(k)}, \mathbf{x}^{(k)}) \right) \mathbf{F}(w) - \frac{6\pi a}{A\, H} \mathbf{R} \cdot \int_{-\infty}^{w} (w - v) \cdot \mathbf{J} \cdot \mathbf{F}(v)\, \mathrm{d}v = \mathbf{0}, \tag{35}$$

where $w = -z$ is the positive distance from the top layer down the array, and $\mathbf{F}$ is a distributed body force. The integral constraint (31) requires

$$\frac{1}{H} \int_0^{\infty} \mathbf{F}(w)\, \mathrm{d}w = \mu\gamma A\, e + A(p^{-\infty} - p^{+\infty})\, \mathbf{e}_z. \tag{36}$$

Differentiating both sides of (35) twice with respect to w, we derive the differential equation

$$\left(\mathbf{I} - \tfrac{3}{4} a \mathbf{R} \cdot \mathbf{D}(\mathbf{x}_k, \mathbf{x}_k) \right) \frac{\mathrm{d}^2 \mathbf{F}(w)}{\mathrm{d}w^2} - \frac{6\pi a}{A\, H} \mathbf{R} \cdot \mathbf{J} \cdot \mathbf{F}(w) = \mathbf{0}. \tag{37}$$

As the size of the particles becomes smaller, the second term in the first set of parentheses on the left-hand side of (37) becomes negligible, and a solution of the resulting simplified equation that decays to zero as w tends to infinity is given by

$$\mathbf{J} \cdot \mathbf{F}(w) = \mathbf{c} \cdot \exp(-\sigma w) \tag{38}$$

where $\mathbf{c}$ is a vectorial constant whose first two components must be evaluated by requiring the satisfaction of the x and y components of the force balance (36), and $\boldsymbol{\sigma}$ is a tensorial rate-of-decay given by

$$\boldsymbol{\sigma}^2 = \frac{6\pi a}{AH}\mathbf{R}. \tag{39}$$

In the case of spherical particles, corresponding to $\mathbf{R} = \mathbf{I}$, this expression is in agreement with that given in Equation (62) of Sangani and Behl [11].

Treating the field (38) as a distributed body force, we now describe the average flow in the semi-infinite matrix in terms of an effective velocity, designated by angular brackets, by means of the equation

$$\mu\mathbf{J} \cdot \frac{\mathrm{d}^2\langle\mathbf{u}\rangle}{\mathrm{d}w^2} + \mathbf{c} \cdot \exp(-\sigma w) = \mathbf{0}. \tag{40}$$

Solving for $\mathbf{J} \cdot \langle\mathbf{u}\rangle$, and expressing the exponential term on the right-hand side in terms of the solution, we obtain the standard form of Brinkman equation for flow in an anisotropic medium

$$\mathbf{J} \cdot \left(\frac{\mathrm{d}^2\langle\mathbf{u}\rangle}{\mathrm{d}w^2} - \sigma^2 \cdot \langle\mathbf{u}\rangle \right) = \mathbf{0}. \tag{41}$$

4. Numerical results for arbitrary particle sizes

To study flow over particles with arbitrary shape and size, we solve the integral Equation (15) using a boundary element method. In the numerical procedure, the surface of a particle is discretized into a collection of six-node curved triangles generated by successively subdividing an octahedron into four descendant elements. The three components of the traction are approximated with constant functions over each element, and the integral equation is evaluated at collocation points located at the centroid of each triangle to produce a system of linear algebraic equations. The Green's function is integrated using the seven-point triangle quadrature over the nonsingular elements [20].

To compute the integral over a singular triangle, we subdivide the triangle into four flat triangles defined by the vertex and mid-nodes, and then integrate individually over each flat triangle in local polar coordinates centered at the singular point. The vector of unknowns includes the three Cartesian components of the traction over each element, and the two components of the slip velocity. Two additional equations arise by appending to the linear system the discrete forms of the x and y components of the integral force balance expressed by the global constraint (6).

It is well known that the integral Equation (15) has an infinite number of solutions: conservation of mass for the flow induced by a lattice of point forces requires

$$\int_{\text{Particle}} n_j(\mathbf{x}) G_{ji}(\mathbf{x}, \mathbf{x}_0)\, \mathrm{d}S(\mathbf{x}) = 0. \tag{42}$$

Because of this identity, any particular solution of the integral Equation (15) may be enhanced with an arbitrary multiple of the normal vector. Combining identity (42) with (12), and using the divergence theorem, we find the reciprocal identity

$$\int_{\text{Particle}} \left(\gamma z e_j + U_j^{+\infty} \right) n_j(\mathbf{x}) \, \mathrm{d}S(\mathbf{x}) = 0. \tag{43}$$

Projecting both sides of (15) onto the normal vector, integrating over the particle surface, and using identity (43), we derive the solvability condition

$$\int_{\text{Particle}} \left(\gamma z e_j + U_j^{+\infty} \right) n_j(\mathbf{x}) \, \mathrm{d}S(\mathbf{x}) = 0 \tag{44}$$

whose satisfaction can be demonstrated readily by use of the divergence theorem.

The non-uniqueness of solution of the integral equation causes the numerical solution of the discretized system to be sensitive to the numerical or round-off error: the more accurate the numerical solution, the higher the condition number of the matrix resulting from the boundary-element discretization. To remove this sensitivity, we consider the discrete form of the integral identity (42) corresponding to the discretization of the integral equation, and express it in the symbolic form

$$\mathbf{A} \cdot \boldsymbol{w} = \mathbf{0}. \tag{45}$$

The discrete approximate eigenvector $\boldsymbol{w}$ contains the components of the normal vector evaluated at the collocation points. If the boundary elements were flat triangles, in which case the discretized particle surface would be polyhedral, the normal vector over each element would be constant, and condition (45) would be satisfied up to the numerical error associated with the numerical computation of the influence matrix $\mathbf{A}$. More generally, $\boldsymbol{w}$ tends to become an exact eigenvector as the discretization error is reduced by increasing the number of the elements.

To the author's knowledge, with a recent exception [21], in all previous numerical solutions of the present or similar integral equations, the nearly-singular behavior of the linear system was ignored, and the numerical method relied on the discretization error, the round-off error, or an inherent geometrical symmetry to produced a sensible solution. General methods for regularizing nearly singular algebraic systems by spectrum deflation have been discussed by several authors in a more general framework [22, 23]. In the present case, the availability of the adjoint eigenvectors of the single-layer potential corresponding to the null eigenvalue allows us to perform regularization with the least amount of perturbation, as follows.

The discrete form of the solvability condition (44) corresponding to the discretization underlying the system (15) is

$$\sum_k (\gamma \; z \; e_i + U_i^{+\infty})_k \, n_i^{(k)} h_k = 0, \tag{46}$$

where summation is implied over $i = 1, 2, 3$, the index k runs over the collocation points, and h_k is an integration weight with respect to surface area playing the role of a discrete metric. In the present implementation, h_k is the element surface area.

To regularize system (45), we multiply both sides by the preconditioning matrix $\mathbf{P}$ defined as

$$\mathbf{P} = \mathbf{I} - \boldsymbol{v}^T \boldsymbol{v}, \tag{47}$$

where the length of the vector $\boldsymbol{\nu}$ is equal to three times the total number of collocation points, and the entries of $\boldsymbol{\nu}$ host the discrete adjoint eigenvector $\alpha n_i^{(k)} h_k$; α is a scaling coefficient adjusted so that the length of $\boldsymbol{\nu}$ is equal to unity. It is evident that $\boldsymbol{\nu}$ is an exact eigenvector of the transpose of the preconditioned singular matrix corresponding to the zero eigenvalue, and the solvability condition is also satisfied to machine accuracy. Thus, the projection guarantees the satisfaction of both the integral identity (43) and the solvability condition (45), while introducing the mildest possible perturbation of the right-hand side: when (43) is fulfilled, the projection has no effect on the right-hand side.

To obtain one solution of the singular preconditioned system, we set the value of the z component of the traction at the last collocation point equal to an arbitrary value that was selected to be zero. Discarding the corresponding equation, we obtain a reduced system with a unique solution that may be computed using any dense-system linear solver, for example, by the method of Gauss elimination.

All computations reported in this section were carried out with 128 boundary elements corresponding to the second level of discretization of the regular octahedron. The sums in real and reciprocal wave number space involved in the computation of the Green's function were truncated at the value of 10. Each solution of the integral equation required several hours of CPU time on a SUN SPARCstation 20, with the majority of the computational effort devoted to evaluating the doubly-periodic Green's function. To estimate the magnitude of the numerical error, the numerical procedure was used to compute flow past a triply periodic array of spheres, by replacing the doubly-periodic Green's function with the triply-periodic Green's function computed in terms of Ewald sums [18]. Comparison with results published by Zick and Homsy [24] for uniform flow through a triply-periodic lattice of spheres showed that the numerical error is less than 0.5% for all reported cases.

In Figure 3(a), we plot with circles and squares, respectively, the slip and drift velocity for shear flow over a square lattice of spherical particles of radius a, where the flow is directed along the x or y axis. The solid line represents the predictions of the asymptotic expression (28), yielding

$$\mathbf{U}^{+\infty} = \mathbf{U}^{-\infty} \cong \gamma L \frac{1}{6\pi} \frac{L}{a} (\alpha - 4{\cdot}39 \, \frac{a}{L}) \mathbf{e}, \tag{48}$$

where L is the length of the base vectors, and $\alpha = 1$. The agreement between the asymptotic and numerical results is excellent up to $a/L = 0{\cdot}15$, at which point the magnitudes of the slip and the drift velocity have become very small. The slip velocity becomes negative when the particle radius exceeds a certain threshold, whereas the drift velocity remains positive for all particle sizes considered. Inversion in the sign of the slip velocity was reported previously by Larson and Higdon [9, 10] and Sangani and Behl [11], respectively, for shear flow over a semi-infinite lattice of cylinders or spheres.

In Figure 3(b), we present corresponding results for shear flow over a hexagonal lattice of spherical particles corresponding to the base vectors $\mathbf{a}_1 = L(1, 0, 0)$, $\mathbf{a}_2 = L\,(0{\cdot}5, 3^{1/2}/2, 0)$. The solid line represents the predictions of the asymptotic expression (28), yielding

$$\mathbf{U}^{+\infty} = \mathbf{U}^{-\infty} \cong \gamma L \frac{0.866}{6\pi} \frac{L}{a} (1 - 4{\cdot}74 \, \frac{a}{L}) \, \mathbf{e}. \tag{49}$$

As in the case of the square lattice, the agreement between the numerical and asymptotic results is surprisingly good even when the particles are not small. In spite of some quantitative differences, the results for the square and the hexagonal lattice are generally similar.

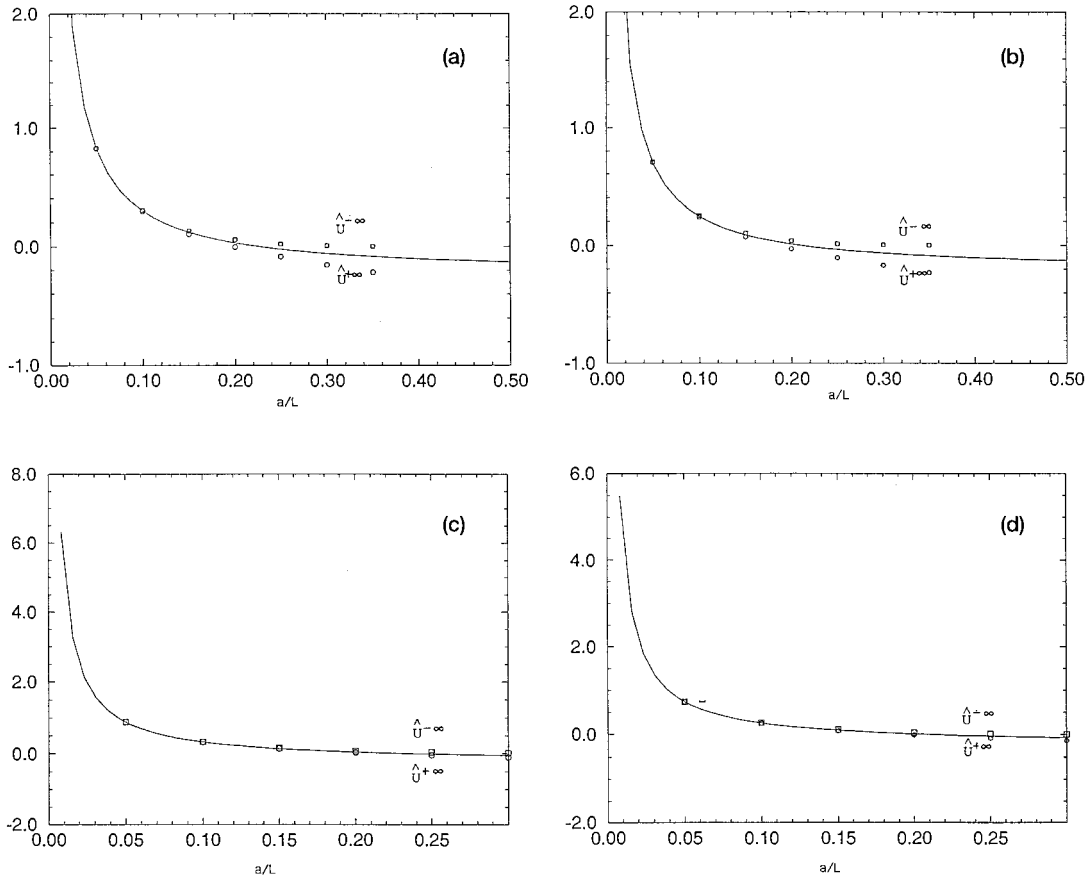

Figure 3. Slip and drift velocity plotted, respectively, with circles and squares for (a) a square lattice of spherical particles of radius a, (b) a hexagonal lattice of spherical particles of radius a, and (c, d) a square lattice of spheroidal particles of aspect ratio 2:1 and equivalent radius a. Panel (c) shows results for flow along the major axis, and panel (d) results for flow along the minor axis. The solid lines represent the predictions of the asymptotic theory for small particle sizes.

In Figure 3(c, d), we present results for shear flow over a square lattice of spheroidal particles with axes ratio 2:1 and equivalent volume radius a, positioned with the major axis parallel to the x axis. The solid lines represent the predictions of the asymptotic expression (28) yielding Equation (48) with $\alpha = 1{\cdot}046$ in the case of flow along the major axis, and $\alpha = 0{\cdot}914$ in the case of flow along the minor axis. The agreement between the asymptotic and numerical results is excellent even for small particle separations. The numerical results show once again that the slip velocity becomes negative when the equivalent radius a crosses a threshold, whereas the drift velocity remains positive for all cases considered. Similar results were obtained for spheroids with different aspect ratios.

As the size of the particles is increased, the tips of the spheroids touch yielding an array of corrugated cylinders. The structure of the flow in this limit may be studied in the context of flow over a periodic array of cylinders, to be discussed in Section 6. The results will show that a negative slip velocity may be established for highly elongated and closely spaced particles due to the onset of regions of recirculating flow in the intervening spaces.

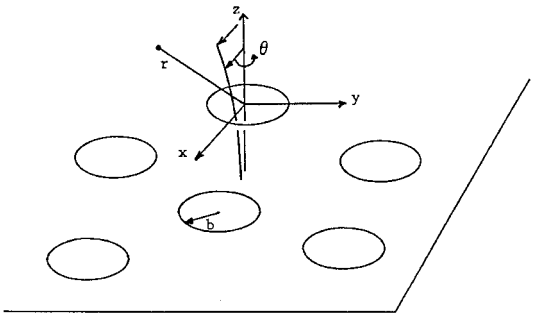

Figure 4. Schematic illustration of shear flow over a flat plate of zero thickness containing a homogeneous distribution of circular perforations.

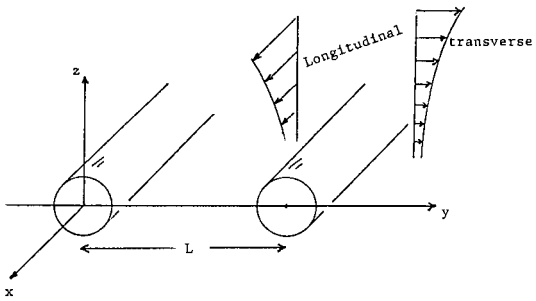

Figure 5. Schematic illustration of longitudinal or transverse shear flow over an array of evenly-spaced cylinders.

Overall, we found that the asymptotic expansions produce sufficiently accurate results in the regimes where the slip and drift velocities are not negligible compared to γa. In practical terms, the data presented in Figure 3 provide us with a basis for computing the size of particles comprising a sieve or membrane in terms of measured values of the drift velocity.

5. Flow over a perforated plate

In the preceding sections, we have discussed flow over a planar lattice of particles of small and moderate size. When the particle size is large, the lattice resembles a plane wall with a periodic distribution of protrusions separated by gaps or perforations. To study the structure of the flow in this limit, we consider a model configuration consisting of an infinite plate of zero thickness with a homogeneous distribution of identical circular perforations separating two semi-infinite domains, and evaluate the drift velocity as a function of the areal fraction of the perforations. The results of Section 2 ensure that the slip and drift velocity will be identical.

When the radius of the perforations is small compared to the distance between any two neighboring perforations, the flow may be expressed as the sum of the incident shear flow and the disturbance flows due to the individual perforations. The building block for generating the latter is the simple shear flow over a circular orifice on a plane wall derived by Smith [12] and Davis [13]. In the Cartesian and accompanying polar coordinates defined in Figure 4, with $\theta = 0$ corresponding to the first quadrant of the zx plane, the velocity components for shear flow along the x axis over a circular orifice of radius b are given by

$$u_x = \gamma \left(f_1 \cos 2\theta + f_2 + \frac{1}{2}(1 + \frac{z}{|z|})z \right), \quad u_y = \gamma f_1 \sin 2\theta, \quad u_z = \gamma f_3 \cos\theta \tag{50}$$

where γ is the shear rate of the overpassing shear flow. We have introduced the auxiliary functions

$$f_1 = \frac{1}{3\pi}\frac{\lambda^2}{b}\zeta\frac{1-\zeta}{(\xi^2+1)(\xi^2+\zeta^2)},$$

$$f_2 = \frac{1}{\pi}b\zeta\left(1-\frac{|\lambda|}{b}\arctan(\frac{b}{|\lambda|}-\frac{1}{3}\frac{\zeta^2}{\xi^2+\zeta^2}\right), \tag{51}$$

$$f_3 = \frac{2}{3\pi}\lambda\zeta\frac{\zeta^2}{\xi^2+\zeta^2}\frac{1-\zeta^2}{1+\xi^2}$$

and we have defined

$$\lambda^2 = \frac{1}{2}\left[r^2-b^2+\left((r^2-b^2)^2+4z^2b^2\right)^{1/2}\right], \quad \lambda = \frac{z}{|z|}|\lambda|, \zeta = \frac{z}{\lambda}, \quad \xi = \frac{\lambda}{b}. \tag{52}$$

The flow in the lower half-plane is the mirror image of the disturbance flow in the upper half-plane. As the distance from the center of the orifice r tends to infinity, the functions f_1, f_2, f_3 tend to vanish. In this limit, $|\lambda|$ tends to r, and the function f_2 assumes the asymptotic form

$$f_2 = \frac{1}{\pi}b\frac{z}{r}\left(1-\frac{r}{b}\arctan\left(\frac{b}{r}\right)-\frac{1}{3}\left(1+\frac{r^4}{z^2b^2}\right)^{-1}\right). \tag{53}$$

As z tends to positive or negative infinity, the infinite sum of the variables expressing the superposition of the individual components of the disturbance velocity reduces to an area integral. Inspecting the expressions given in (50), we find that the assumption of a homogeneous distribution of perforations requires that all integral vanish, with the exception of the integrals of the function f_2 corresponding to the direction of the shear flow. Considering the limit as z tends to positive or negative infinity, we use the asymptotic form (53) and obtain

$$\begin{aligned} u_x \to u_x^{\pm\infty} = {} & \gamma\frac{1-\phi}{b^2}\lim_{z\to\infty}2\pi\int_0^\infty\frac{1}{\pi}b\frac{z}{(z^2+\rho^2)^{1/2}}\left(1-\frac{(z^2+\rho^2)^{1/2}}{b}\right. \\ & \left.\arctan\left(\frac{b}{(z^2+\rho^2)^{1/2}}\right)\right)-\frac{1}{3}\left(1+\frac{(z^2+\rho^2)^2}{z^2b^2}\right)\rho\,\mathrm{d}\rho+\gamma\frac{1}{2}\left(1+\frac{z}{|z|}\right)z, \end{aligned} \tag{54}$$

where $1-\phi$ is the areal fraction of the perforations. Taking the limit as z tends to infinity while the ratio ρ/z remains finite, we find the asymptotic expression

$$u_x^{\pm\infty}-\gamma\frac{1}{2}(1+\frac{z}{|z|}) = \frac{2}{3}(1-\phi)\gamma b\int_0^{\pi/2}\sin^3\omega\,\mathrm{d}\omega = \frac{4}{9}(1-\phi)\gamma b = \frac{4\pi}{9}n\gamma b^3 \tag{55}$$

which is valid when the solid areal fraction ϕ of the plate is sufficiently close to unity and the perforations are separated by a great distance; n on the right-hand side is the number density of the perforations defined as the number of perforations per unit area of the plate.

To compare expression (55) with the diametrically opposite expansion (29) corresponding to the limit of small solid fractions, we set $b = a((1-\phi)/\phi)^{1/2}$, and find

$$u_x^{\pm\infty}-\gamma\frac{1}{2}(1+\frac{z}{|z|})z = U_x^{+\infty} = \frac{4}{9}\gamma a\frac{(1-\phi)^{3/2}}{\phi^{1/2}}. \tag{56}$$

It is evident that different functional forms arise in the asymptotic limit of ϕ tending to zero or to unity.

Previous numerical solutions have shown that the structure of shear flow over a solitary orifice with non-zero thickness is sensitive to the thickness of the plate hosting the orifice, and this suggests that the drift and slip velocity will be strong functions of the plate thickness. Indeed, the numerical solutions presented in Section 4 revealed that the slip velocity becomes negative for sufficiently large values of ϕ, whereas (56) predicts positive values.

6. Shear flow over an array of cylinders

The formulation of the preceding sections may be extended in a straightforward fashion to describe shear flow over a periodic array of cylinders separated by the distance L, modeling, for example, a membrane consisting of elongated fibers, as depicted in Figure 5. A shear flow in an arbitrary direction may be decomposed into a unidirectional longitudinal flow along the x axis parallel to the generators, and a transverse flow along the y axis normal to the generators. Both the longitudinal and the transverse flow over a semi-infinite regular lattice were discussed by Larson and Higdon [9, 10]. Their results illustrated the structure of the streamline patterns and established the dependence of the slip velocity on the cylinder shape and areal fraction.

6.1. Integral formulation

Considering first the case of longitudinal flow, we work as in Section 2 and derive the integral representation

$$u_x(\mathbf{X}_0) = -\frac{1}{\mu}\int_{\text{Cylinder}} G^L(\mathbf{x},\mathbf{x}_0)\, f_x(\mathbf{x})\, \mathrm{d}l(\mathbf{x}) + \gamma z_0 + U_x^{+\infty}, \tag{57}$$

where the integral is over the contour of one cylinder in the yz plane, l is the arc length, and f_x is the x-component of the traction. The kernel G^L is the upward biased singly-periodic Green's function of Laplace's equation given by

$$G^L(\mathbf{x},\mathbf{x}_0) = \frac{1}{2\pi}H(\mathbf{x},\mathbf{x}_0) - \frac{1}{2}\frac{z-z_0}{L}, \tag{58}$$

where

$$H(\mathbf{x},\mathbf{x}_0) = -\frac{1}{2}\log\left[2\cosh\left(\frac{2\pi}{L}(z-z_0)\right) - 2\cos\left(\frac{2\pi}{L}(y-y_0)\right)\right] \tag{59}$$

representing the harmonic potential at the point $\mathbf{x}$ due to a periodic array of two-dimensional point sinks of unit strength, where one of the point sinks is located at the point $\mathbf{x}_0$. Far above the array of point sinks, as $z - z_0$ tends to $+\infty$, the Green's function exhibits the asymptotic behavior $G^L \to -(z-z_0)/L + \text{edt}$; far below the array, as $z - z_0$ tends to $-\infty$, the Green's function vanishes at an exponential rate. Using these conditions, we find that the slip and drift velocity are related by

$$U_x^{-\infty} = U_x^{+\infty} + \frac{1}{\mu L}\int_{\text{Cylinder}} z\; f_x(\mathbf{x})\, \mathrm{d}l(\mathbf{x}). \tag{60}$$

Considering next the case of transverse flow along the y axis, we work as in Section 2 and derive the integral representation

$$u_j(\mathbf{x}_0) = -\frac{1}{4\pi\mu}\int_{\text{Cylinder}} G_{ij}^{2D-1P}(\mathbf{x},\mathbf{x}_0)\, f_i(\mathbf{x})\, \mathrm{d}l(\mathbf{x}) + \delta_{jy}\,\gamma\, z_0 + \delta_{jy} U_y^{+\infty} \tag{61}$$

where the indices i and j range over y and z, and G_{ij}^{2D-1P} is the singly-periodic Green's function of Stokes flow with components

$$\begin{aligned} G_{yy}^{2D-1P}(\mathbf{x},\mathbf{x}_0) &= H(\mathbf{x},\mathbf{x}_0) + (z-z_0)\frac{\partial H(\mathbf{x},\mathbf{x}_0)}{\partial z} - 2\pi\frac{z-z_0}{L}, \\ G_{yz}^{2D-1P}(\mathbf{x},\mathbf{x}_0) &= G_{zy}^{2D-1P}(\mathbf{x},\mathbf{x}_0) = -(z-z_0)\frac{\partial H(\mathbf{x},\mathbf{x}_0)}{\partial y}, \\ G_{zz}^{2D-1P}(\mathbf{x},\mathbf{x}_0) &= H(\mathbf{x},\mathbf{x}_0) + (z-z_0)\frac{\partial H(\mathbf{x},\mathbf{x}_0)}{\partial z} \end{aligned} \tag{62}$$

representing the velocity due to an array of two-dimensional point forces. The streamline pattern established when the point forces are directed parallel to the array is depicted in Figure 2(b). Far above the array of the point forces, as $z - z_0$ tends to $+\infty$, $G_{xx}^{2D-1P} \to -4\pi(z-z_0)/L + \text{edt}$, while the other components decay at an exponential rate. Far below the array, as $z - z_0$ tends to $-\infty$, all components of G_{ij}^{2D-1P} decay at an exponential rate. Using these conditions, we find that the slip and drift velocities are related by

$$U_y^{-\infty} = U_y^{+\infty} + \frac{1}{\mu L}\int_{Particle} z\, f_y(\mathbf{x})\, \mathrm{d}l(\mathbf{x}). \tag{63}$$

As in the case of three-dimensional flow, the difference between these two velocities is on the order of the cylinder size normal to the array.

6.2. Asymptotics for small circular cylinders

The ill-posedness of infinite two-dimensional Stokes flow prevents us from using the method of matched asymptotic expansions to derive expressions for the slip and drift velocity in the limit of small cylinder sizes. Hasimoto [25] modified a method pioneered by Burgers to study uniform flow through a doubly-periodic array of circular cylinders of small size. The method involves writing the integral representation (57) or (61) at a point on the surface of a cylinder, expanding the Green's function into a Laurent series whose leading term is the free-space Laplace Green's function or the two- dimensional Stokeslet, retaining only the singular and constant terms, and then requiring that the integral of the velocity over the contour of the cylinder vanish. Hasimoto [25], Sangani and Acrivos [26], and Drummond and Tahir [27] confirmed the validity of this approach by recomputing and extending the asymptotic expansion using different methods.

Applying Burgers' method to the present problem, we find

$$U^{\pm\infty} \cong \frac{\gamma L}{2\pi}\left(-\log\left(\frac{a}{L}\right) - 1{\cdot}879\right) \tag{64}$$

for longitudinal flow, and

$$U^{\pm\infty} \cong \frac{\gamma L}{4\pi}\left(-\log\left(\frac{a}{L}\right) - 2{\cdot}3379\right) \tag{65}$$

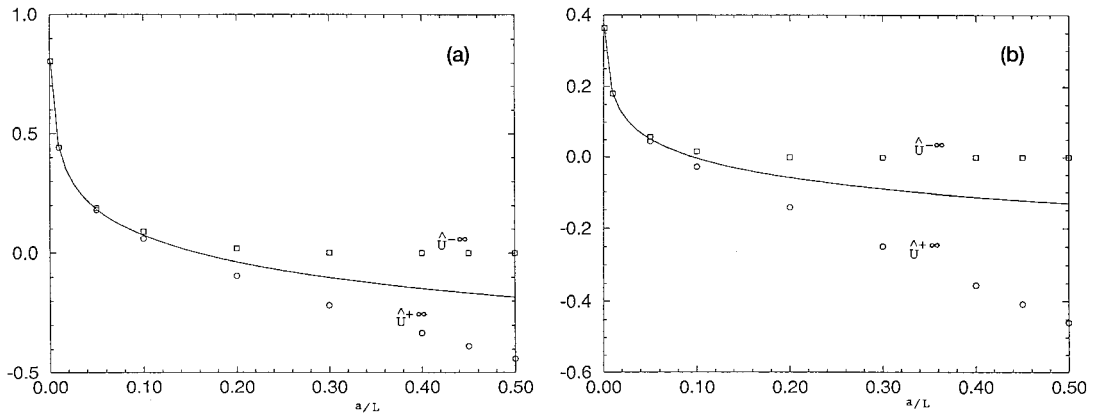

Figure 6 Slip and drift velocity plotted, respectively, with circles and squares for (a) longitudinal, and (b) transverse flow past an array of cylinders of radius a separated by the distance L.

for transverse flow. The logarithmic dependence may be contrasted with the inverse first power behavior encountered previously for three-dimensional flow, underscoring once more the distinct nature of two- and three-dimensional Stokes flow.

6.3. Numerical results for circular cylinders

The integral equations arising from the integral representations (57) and (61) were solved using the counterpart of the numerical method discussed in Section 4. In Figure 6(a, b), we plot, respectively, with circles and squares the slip and drift velocity for longitudinal and transverse flow past an array of cylinders of radius a separated by the distance L; the caret indicates nondimensionalization with respect to γL. The solid lines represent the predictions of the asymptotic expressions (64) and (65). In both cases, the numerical results confirm that as a/L tends to vanish, both velocities diverge at a logarithmic rate. Significant differences between the asymptotic predictions and the numerical results arise when a/L becomes approximately greater than 0·10.

For small cylinder sizes, the slip and drift velocities are positive for both longitudinal and transverse flow. As the cylinders become larger, the slip velocity becomes negative at a certain cylinder radius. In the limit as a/L tends to 0·5, corresponding to touching cylinders, the slip velocity tends to a limiting value that is consistent with a value extrapolated from graphs presented by Larson and Higdon [9, 10] for shear flow over a semi-infinite lattice. To make this comparison, we recomputed the slip velocity in terms of the flow rate above the array, as discussed by the previous authors. In the case of longitudinal flow, the drift velocity is positive for any cylinder radius, in agreement with physical intuition. In the case of transverse flow, however, as the cylinders become larger, the drift velocity changes sign at a particular cylinder radius and then it shows weak fluctuations.

To explain the physical reason for a negative drift velocity, in Figure 7(a, b) we present streamline patterns for $a/L = 0{\cdot}10$ and 0·30. In the first case, regions of recirculating flow do not develop, and the fluid moves in the direction of the shear flow above and below the array. To demonstrate the effect of the cylinder geometry, in Figure 7(c) we present the streamline pattern for flow over a plane wall with a slit, computed using the exact solution derived by Smith [12]. The comparison reveals topologically similar features near the opening, but significant differences below the plate due to the establishment of the drift velocity in the case

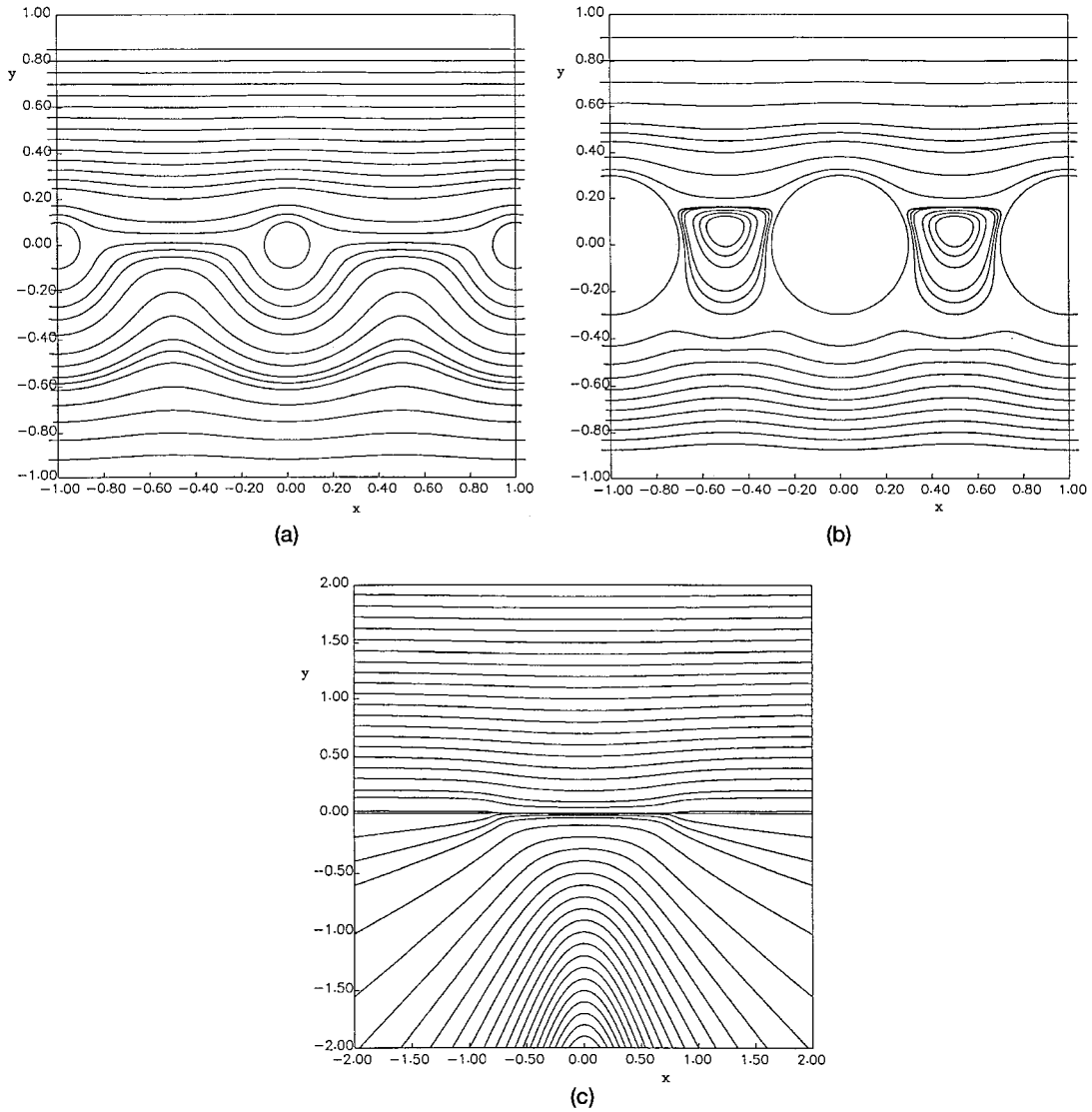

Figure 7 Streamline patterns for shear flow over an array for circular cylinders for (a) $a/L = 0{\cdot}10$ and (b) $0{\cdot}30$. Streamline patterns for shear flow over a plane wall with a slit.

of flow over the cylinders. Figure 7(b) reveals that when $a/L = 0{\cdot}30$, regions of recirculating flow develop between the cylinders. The backward motion of the fluid at the bottom of the eddies drives a weak flow with a negative drift velocity.

7. Concluding remarks

We have studied shear flow over a planar lattice of particles by asymptotic and numerical methods. The asymptotic results were found to generate accurate predictions over an extended range of particle sizes in the case of three-dimensional flow, and over a moderate range of particle sizes in the less realistic case two-dimensional flow. We have also derived asymptotic expressions for the slip and drift velocity of shear flow over a plate with a homogeneous

distribution of perforations, in the limit of large solid fractions. These expressions are suitable for deriving modified boundary conditions that relate the local jump in the shear stress to the jump in the velocity across a membrane subjected to an ambient flow.

The model problems considered in this study involve flow over regular arrays. In reality, the particles are likely to be distributed randomly over the plane of the array. The hydrodynamical laws of flow through random particulate media and over random porous surfaces have been shown to be fundamentally different from those for ordered media, at least in the limit of small volume fractions [28–30]. Accordingly, the slip and drift velocities of flow over regular arrays are expected to obey laws that are different than those for random arrays in the limit of small particle sizes. Whether or not the dichotomy persists at higher solid fractions needs to be addressed in future analysis.

Acknowledgement

This research has been supported by a grant provided by the National Science Foundation.

References

1. R. Lipowsky, The conformation of membranes. *Nature* 349 (1991) 475–481.
2. U. Seifert, Configurations of fluid membranes and vesicles. *Adv. in Phys.* 46 (1997) 13–137.
3. R. Lipowsky and E. Sackmann (Eds.), *Structure and Dynamics of Membranes* (Vol I). Amsterdam: Elsevier (1995) 1020 p.
4. H. Yasuda, G.E. Lamaze and A. Peterlin, Diffusive and hydraulic permeabilities of water in water-swollen polymer membranes. *J. Polym. Sci. A* 2 (1971) 1117–1131.
5. G. H. Malone, T. E. Hutchinson and S. Prager, Molecular models for permeation through thin membranes: the effect of hydrodynamic interaction on permeability. *J. Fluid Mech.* 65 (1974) 753–767.
6. K. Ishii, Viscous flow past multiple planar arrays of small spheres. *J. Phys. Soc. Japan* 46 (1979) 675–680.
7. E. O. Tuck and A. Kouzoubov, A laminar roughness boundary condition. *J. Fluid Mech.* 300 (1995) 59–70.
8. K. Sarkar and A. Prosperetti, Effective boundary conditions for Stokes flow over a rough surface. *J. Fluid Mech.* 312 (1996) 1–19.
9. R. E. Larson and J. J. L. Higdon, Microscopic flow near the surface of two-dimensional porous media. Part 1. Axial flow. *J. Fluid Mech.* 166 (1986) 449–472.
10. R. E. Larson and J. J. L. Higdon, Microscopic flow near the surface of two-dimensional porous media. Part 2. Transverse flow. *J. Fluid Mech.* 178 (1987) 119–136.
11. A. S. Sangani and S. Behl, The planar singular solutions of Stokes and Laplace equations and their application to transport processes near porous surfaces. *Phys. Fluids A* 1 (1989) 21–37.
12. S. H. Smith, Stokes flow past slits and holes. *Int. J. Multiphase Flow* 13 (1987) 219–231.
13. A. M. J. Davis, Shear flow disturbance due to a hole in the plane. *Phys. Fluids A*3 (1991) 478–480.
14. Z.-Y. Yan, A. Acrivos and S. Weinbaum, Fluid skimming and particle entrainment into a small circular side pore. *J. Fluid Mech.* 229 (1991) 1–27.
15. W.-Y. Wu, S. Weinbaum and A. Acrivos, Shear flow over a wall with suction and its application to particle screening. *J. Fluid Mech.* 243 (1992) 489–518.
16. 24 G. S. Beavers and D. D. Joseph, Boundary conditions at a naturally permeable wall. *J. Fluid Mech.* 30 (1967), 197–207.
17. C. Pozrikidis, *Boundary Integral and Singularity Methods for Linearized Viscous Flow.* Cambridge: Cambridge University Press (1992) 25 p.
18. C. Pozrikidis, Computation of periodic Green's functions of Stokes flow. *J. Eng. Math.* 30 (1996) 79–96.
19. P. G. Saffman, On the settling speed of free and fixed suspensions. *Stud. Appl. Math.* 52 (1973) 115–127.
20. C. Pozrikidis, *Numerical Computation in Science and Engineering.* New York: Oxford University Press, (1998) 62 p.
21. C. Pozrikidis, A spectral-element method for particulate Stokes flow. *J. Comp. Phys.* 156 (1999) 360–381.

22. T. F. Chan, Deflated decomposition of solutions of nearly singular systems. *SIAM J. Numer. Anal.* 21 (1984) 738–745.
23. P. C. Hansen, *Rank-deficient and Discrete Ill-posed Problems*. Philadelphia: *SIAM* (1997) 24 p.
24. A. A. Zick and G. M. Homsy, Stokes flow through periodic arrays of spheres. *J. Fluid Mech.* 115 (1982) 13–26.
25. H. Hasimoto, On the periodic fundamental solutions of the Stokes equations and their application to viscous flow past a cubic array of spheres. *J. Fluid Mech.* 5 (1959) 317–328.
26. A. S. Sangani and A. Acrivos, Slow flow through a periodic array of spheres. *Int. J. Multiphase Flow* 8 (1982) 343–360.
27. J. E. Drummond and M. I. Tahir , Laminar viscous flow through regular arrays of parallel solid cylinders. *Int. J. Multiphase Flow* 10 (1984) 515–540.
28. P. G. Saffman, On the boundary condition at the surface of a porous medium. *Stud. Appl. Math.* 50 (1971) 93–101.
29. I. D. Howells, Drag due to the motion of a Newtonian fluid through a sparse random array of small fixed rigid objects. *J. Fluid Mech.* 64 (1974) 449–475.
30. A. S. Sangani and C. Yao, Transport processes in random arrays of cylinders. II Viscous flow. *Phys. Fluids* 31 (1988) 2426–2434.